# Cavity Optomagnonics with Spin-Orbit Coupled Photons

A. Osada,[1,*] R. Hisatomi,[1] A. Noguchi,[1] Y. Tabuchi,[1] R. Yamazaki,[1] K. Usami,[1,†] M. Sadgrove,[2,‡] R. Yalla,[2] M. Nomura,[3] and Y. Nakamura[1,4]

[1]*Research Center for Advanced Science and Technology (RCAST), The University of Tokyo, Meguro-ku, Tokyo 153-8904, Japan*
[2]*Center for Photonic Innovation, University of Electro-Communication, Chofu, Tokyo 182-8285, Japan*
[3]*Institute of Industrial Science (IIS), The University of Tokyo, Meguro-ku, Tokyo 153-8505, Japan*
[4]*Center for Emergent Matter Science (CEMS), RIKEN, Wako, Saitama 351-0198, Japan*

(Received 7 October 2015; published 2 June 2016)

We experimentally implement a system of *cavity optomagnonics*, where a sphere of ferromagnetic material supports whispering gallery modes (WGMs) for photons and the magnetostatic mode for magnons. We observe pronounced nonreciprocity and asymmetry in the sideband signals generated by the magnon-induced Brillouin scattering of light. The spin-orbit coupled nature of the WGM photons, their geometrical birefringence, and the time-reversal symmetry breaking in the magnon dynamics impose the angular-momentum selection rules in the scattering process and account for the observed phenomena. The unique features of the system may find interesting applications at the crossroad between quantum optics and spintronics.

DOI: 10.1103/PhysRevLett.116.223601

Spin-orbit coupling of electrons is responsible for many phenomena in condensed matter physics, such as spin-orbit splitting of the band structure [1], the spin-Hall effect [2], and topological insulators [3]. Photons also have angular and polarization (spin) degrees of freedom, and in most cases they can be treated independently. However, the approximation breaks down when the spatial structure of the light mode becomes comparable to the wavelength. In such a case, inseparability of the orbital and spin degrees of freedom, or the spin-orbit coupling of photons, manifests itself. While this was pointed out in the literature such as Ref. [4], it took some time before researchers acknowledged its usefulness [5–7]. Recently, the spin-orbit coupled nature of photons was vividly demonstrated in a gold nanoparticle on an optical nanofiber [8] and laser-cooled Cs atoms in the vicinity of the surface of a whispering gallery mode (WGM) resonator [9]. The distinct nature of the spin-orbit coupling associated with WGMs is that the light circulating in one direction corresponds to $\sigma^+$ polarization and the other to $\sigma^-$, with respect to the direction perpendicular to the plane of the WGM orbit [9]. WGM resonators have also been intensively studied in the regime of small mode volume and the high quality factor allowing the enhancement of nonlinear optical effects [10–13].

Here we demonstrate intriguing properties of spin-orbit coupled photons interacting with collective spin excitations in a millimeter-scale ferromagnetic sphere. By modifying the probability of the Brillouin scattering through WGMs, one can realize cavity-assisted manipulations of magnons, leading to a new field of cavity optomagnonics, in much the same spirit as the cavity optomechanics [12]. An additional novel feature in cavity optomagnonics is the chirality provided by the spin dynamics in the ferromagnet. This leads not only to magnon-induced nonreciprocal Brillouin scattering but also to the creation and annihilation of magnons in a highly selective manner, with the linear-polarization input. Moreover, WGMs coupled via an optical nanofiber will allow us to employ the resonant structures for the enhancement of the Brillouin scattering. The combination of these properties, which was absent in the previous works [14,15], provide a new, complementary way to investigate the magnon-induced Brillouin scattering. We note that recent works in similar setups also observed inelastic [16] and elastic [17] scattering of light by the ferromagnetic spins. It has also been shown that magnons in ferromagnets can be coherently coupled to a microwave cavity mode [18] as well as a superconducting qubit [19] in the quantum regime. Thus, the system of cavity optomagnonics presented here can open a way to optically control these degrees of freedom in the future. (We also note that, in a separate work, the authors studied the bidirectional microwave-optical conversion using a propagating light mode and a microwave cavity mode coupled to magnons [20].)

A schematic of our experimental setup is shown in Fig. 1(a). The WGM resonator we use is a 750-$\mu$m-diameter sphere made of a ferromagnetic insulator, yttrium iron garnet (YIG). YIG is highly transparent at the optical wavelength of 1.5 $\mu$m and has a refractive index of 2.19. With a Curie temperature of about 550 K, YIG is in the ferromagnetic phase at room temperature and supports long-wavelength magnetostatic modes [21]. We focus, in particular, on the Kittel mode with spatially uniform spin precession, which exhibits a sharp ferromagnetic resonance (FMR) [18]. In order to saturate the magnetization and to define the quantization axis, a dc magnetic field $B$ of 0.24 T

 

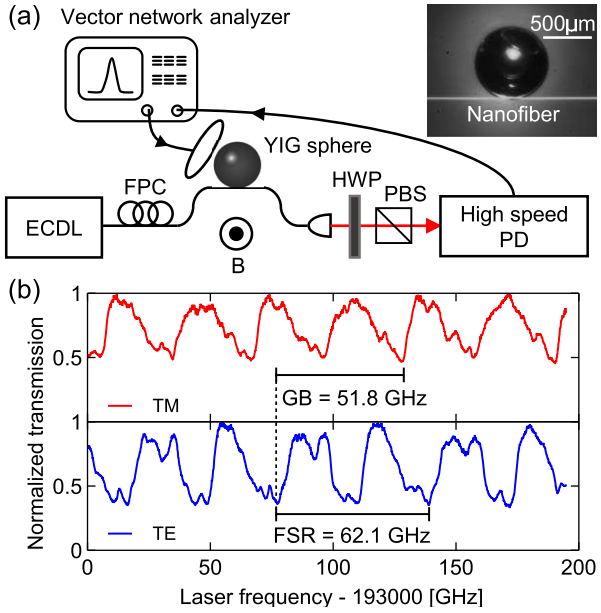


FIG. 1. Transmission through WGMs in a YIG sphere. (a) Experimental setup. WGMs of the YIG sphere are addressed with an optical nanofiber. Microwave radiation from a vector network analyzer excites magnons, and ac and dc components of the light intensity are monitored with a high-speed photodetector (PD). The polarization of the light from an external-cavity diode laser (ECDL) is adjusted by a fiber polarization controller (FPC). A half-wave plate (HWP) and a polarization beam splitter (PBS) are placed before the PD. The inset shows a picture of the YIG sphere and the nanofiber. (b) Observed WGM spectra for the 750-$\mu$m-diameter YIG sphere. Red and blue lines correspond to the TM and TE modes, respectively. The transmission signals are normalized by their maximal values. The free spectral range (FSR) and the estimated spectral shift due to the geometrical birefringence (GB) are indicated.

is applied perpendicular to the plane of the WGM orbits. A loop coil near the YIG sphere generates an ac magnetic field perpendicular to the dc field and drives FMR. The magnetization then acquires its horizontal component rotating at the angular frequency of the Kittel mode. Because of the finite loss, the microwave reflection picked up by the loop coil shows a dip at the resonant frequency. The resonant frequency and the quality factor are found to be $\omega_{\rm mag}/2\pi = 6.81$ GHz and $Q \sim 3000$, respectively.

Laser light with a wavelength of 1.5 $\mu$m from an ECDL is introduced through a FPC and then coupled to the WGM resonator via a tapered silica optical nanofiber, with a waist diameter of about 700 nm and a waist length of around 4 mm. Figure 1(b) shows the transmission spectra for the transverse-electric (TE) modes and the transverse-magnetic (TM) modes. The rich structures in the spectra indicate that there are various spatial modes within the FSR of 62.1 GHz. For WGMs in the large sphere limit, frequencies of the TM modes are known to be higher than those of the TE modes with the same mode indices because of the geometrical birefringence [22–24]. For the 750-$\mu$m-diameter sphere we use, the difference is estimated to be 51.8 GHz, which is consistent with the observed spectra in Fig. 1(b) [25]. The intrinsic quality factors of the WGMs are found to be around $1 \times 10^5$ when they are measured in the undercoupled regime.

When the light propagates in the direction of the mean magnetization in ferromagnets, the well-known Faraday effect occurs. When, on the other hand, the mean magnetization is perpendicular to the direction of light propagation, magnon-induced Brillouin scattering takes place [26–28]. In the presence of magnons in the Kittel mode, photons in the WGM undergo Brillouin scattering to create sideband photons with the frequency shifted by $\pm\omega_{\rm mag}/2\pi$. A HWP and a PBS make the scattered sideband photons and the unscattered input photons interfere to generate a beat signal at $\omega_{\rm mag}/2\pi$. The signal is amplified and measured with a vector network analyzer.

The orange (light blue) plot in Fig. 2 shows the observed spectrum of the beat signal for the input laser being the TM mode and coupled to the anticlockwise (clockwise) orbit of the WGM resonator. The frequency of the input photons is tuned to be $\omega/2\pi = 193130$ GHz where the beat signal associated with the anticlockwise orbit is maximized. While both peaks in Fig. 2 have the same linewidth as the FMR signal, there is a large difference in their signal strengths of almost 20 dB.

The nonreciprocity of the magnon-induced Brillouin scattering can be explained by considering the conservation of energy, momentum, and angular momentum under the situation in which the spin-orbit coupling of the photons and the geometrical birefringence associated with the WGM resonator are blended with the time-reversal symmetry breaking in the magnon dynamics.

Suppose that the input laser polarization is adjusted to couple to the TM mode of the anticlockwise WGM orbit (orange orbit in Fig. 2). The light in the resonator is then $\sigma^+$ polarized due to the spin-orbit coupling [see Fig. 3(a)]. To see why the Brillouin scattering is more noticeable in this situation, we consider the following three points. (i) The

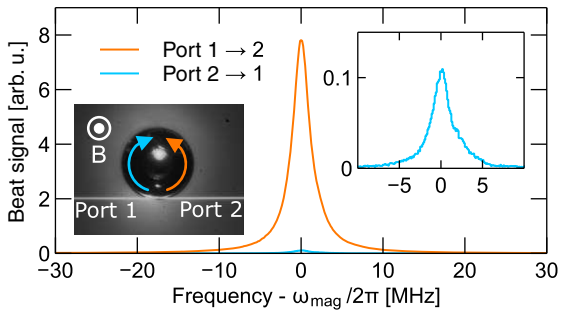


FIG. 2. Nonreciprocal Brillouin scattering. The orange (light blue) plot is the observed spectrum of the beat signal for the input laser being TM mode from port 1 (2). The right inset shows an expanded plot of the light blue curve. The left inset depicts the input ports and the direction of the dc magnetic field.

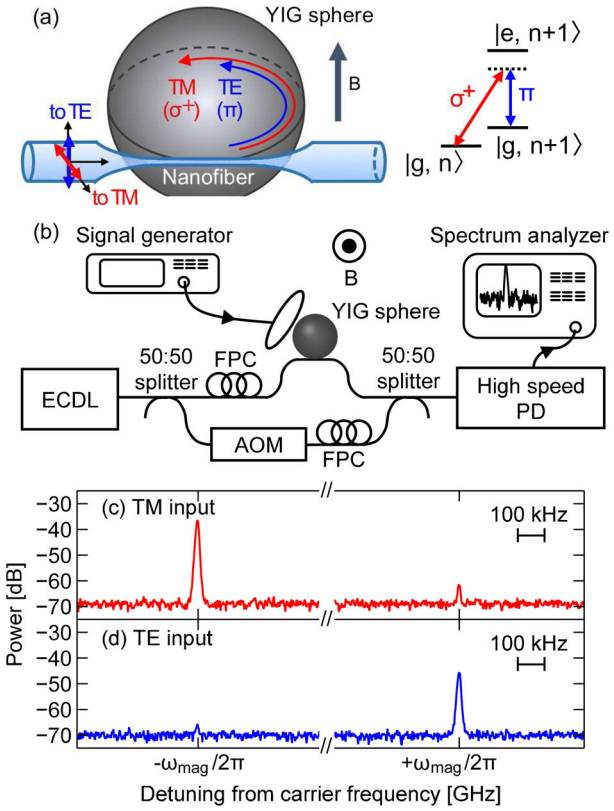


FIG. 3. Sideband asymmetry in magnon-induced Brillouin scattering. (a) Correspondence of input polarizations, polarizations in the WGM resonator, and a schematic level diagram of the Brillouin scattering. (b) Setup for observing individual sidebands. Laser light with a wavelength of 1.5 $\mu$m is split into two paths, and the photons in one of the paths acts as a local oscillator (LO), whose frequency is shifted by 150 MHz by an acousto-optic modulator (AOM). For the heterodyne measurement, the LO photons are mixed with the photons in the other path which are coupled to the WGM resonator via the nanofiber. Microwaves from a signal generator resonantly excite the magnons, and the heterodyne signal is sent to a spectrum analyzer. (c),(d) Observed sideband-signal powers for the TM-mode and TE-mode inputs, respectively, for a laser frequency of 193130 GHz. The resolution bandwidth of the measurement is 10 kHz.

conservation of energy and spin angular momentum constrain the ensuing Brillouin scattering to create a magnon and a sideband photon at the angular frequency of $\omega - \omega_{\mathrm{mag}}$ in the $\pi$-polarized TE mode. Here we assume that the Brillouin scattering occurs only between TM and TE modes with the same WGM index, which means that the orbital angular momentum of photons is conserved. We shall return to this issue later. (ii) Momentum conservation in the Brillouin scattering process with a magnon in the Kittel mode (having zero wave vector) leads to negligible backscattering. This is in stark contrast with the schemes utilizing the phonons with nonzero wave vectors [29–32] and active-passive-coupled microresonators [33,34]. (iii) Since the frequency of the TM mode $\omega_{\mathrm{TM}}$ is larger than that of the TE mode $\omega_{\mathrm{TE}}$ with the same mode index because of the geometrical birefringence (this is true regardless of the circulation direction of the photon [22–24]), the scattering process favors an output TE photon with a lower frequency than that of the input TM photon, which is indeed the case for the anticlockwise orbit.

On the contrary, for the input photons in the clockwise orbit (light blue orbit in Fig. 2) the polarization is $\sigma^-$ and a magnon must be annihilated. The accompanying sideband photon in the TE mode then has to have an angular frequency of $\omega + \omega_{\mathrm{mag}}$, an unfavorable situation from the viewpoint of the geometrical birefringence, $\omega_{\mathrm{TE}} < \omega_{\mathrm{TM}}$. This leads to the suppression of the beat signal for the clockwise photons as shown in Fig. 2. The observed small but finite signal shown in the inset can be due to the imperfection of the spin-orbit coupling associated with the WGM.

To clarify the selection rule in the Brillouin scattering, we consider the states $|g, n\rangle$ and $|e, n\rangle$, describing the electronic ground and excited states of the optical transition, $|g\rangle$ and $|e\rangle$, respectively, and the number of magnons in the Kittel mode, $|n\rangle$. If the input photons are in the TM mode, the light in the resonator is $\sigma^+$ polarized as shown in Fig. 3(a), and thus the state $|g, n\rangle$ is transformed into $|g, n+1\rangle$ via the excited state $|e, n+1\rangle$ by creating a magnon and a down-converted red-sideband photon with $\pi$ polarization in the TE mode. On the other hand, if the input photons are in the TE mode, the light in the resonator is $\pi$ polarized, and the reverse process occurs by annihilating a magnon and creating an up-converted blue-sideband photon with $\sigma^+$ polarization in the TM mode. Note that the dominant optical transition here is considered to be the spin- and parity-allowed ${}^6S(3d^5 2p^6) \leftrightarrow {}^6P(3d^6 2p^5)$ charge transfer transition in YIG [35], whose transition wavelength is around 440 nm. Since the laser wavelength of 1.5 $\mu$m is far detuned from the transition, the excited state $|e\rangle$ is only virtually populated.

To verify the asymmetry in sideband signals produced by the Brillouin scattering, the red- and blue-sideband signals are obtained in a heterodyne measurement. A schematic picture of the experimental setup is shown in Fig. 3(b). With this scheme, the red and blue sidebands are separately observed by the spectrum analyzer at frequencies $\omega_{\mathrm{mag}}/2\pi + 150$ and $\omega_{\mathrm{mag}}/2\pi - 150$ MHz, respectively. The results for the TM-mode input are shown in Fig. 3(c). The blue sideband is suppressed by more than 20 dB relative to the red one. For the TE mode input, the ratio of sideband strengths is reversed as shown in Fig. 3(d). These results imply that, by changing the polarization of the input laser, one can create or annihilate magnons in a highly controlled manner.

So far, we have assumed that the Brillouin scattering occurs only between the TM and TE modes with the same WGM index and thus conserves the orbital angular momentum of the photons. To support this hypothesis,

we further analyze the Brillouin scattering strength for the TE and TM inputs. Let the density of states of a relevant WGM for the TM mode be $\rho_{\mathrm{TM}}^{(i)}(\omega)$ and that for the TE mode be $\rho_{\mathrm{TM}}^{(i)}(\omega)$, where $i$ represents the indices characterizing the WGMs. Suppose that the input photon is in the TE mode with angular frequency $\omega$ and the scattered into the TM mode with $\omega+\omega_{\mathrm{mag}}$. The strength of the Brillouin scattering is then written in the form proportional to the input photon number $n_{\mathrm{TE}}^{(i)}$ and then the density of states of the final state $\rho_{\mathrm{TM}}^{(i)}(\omega+\omega_{\mathrm{mag}})$ [25]. Since $n_{\mathrm{TE}}^{(i)}$ is proportional to $\rho_{\mathrm{TE}}^{(i)}(\omega)$, the scattering strength is written as $I_{\mathrm{TE}\to\mathrm{TM}}(\omega)\equiv\sum_i C_i\rho_{\mathrm{TE}}^{(i)}(\omega)\rho_{\mathrm{TM}}^{(i)}(\omega+\omega_{\mathrm{mag}})$ with coefficient $C_i$ representing the contributions from each mode. For the TM mode input, the same consideration results in $I_{\mathrm{TM}\to\mathrm{TE}}(\omega)\equiv\sum_i C_i\rho_{\mathrm{TM}}^{(i)}(\omega)\rho_{\mathrm{TE}}^{(i)}(\omega-\omega_{\mathrm{mag}})$. Thus, one can immediately see that $I_{\mathrm{TE}\to\mathrm{TM}}(\omega)=I_{\mathrm{TM}\to\mathrm{TE}}(\omega+\omega_{\mathrm{mag}})$.

We measure the laser-frequency dependence of the beat signal in the setup shown in Fig. 1(a) for the TM- and TE-mode inputs. The observed spectra are compared in Figs. 4(a) and 4(b), and indeed we find an apparent similarity. We characterize the similarity between the two spectra by calculating the cross-correlation between them. Here the cross-correlation $R_{\mathrm{TE;TM}}$ is defined as

$$R_{\mathrm{TE;TM}}(\Omega)=\frac{\left(\int_0^\infty\frac{d\omega}{2\pi}\sqrt{I_{\mathrm{TE}\to\mathrm{TM}}^{(\mathrm{exp})}(\omega)I_{\mathrm{TM}\to\mathrm{TE}}^{(\mathrm{exp})}(\omega+\Omega)}\right)^2}{\int_0^\infty\frac{d\omega}{2\pi}I_{\mathrm{TE}\to\mathrm{TM}}^{(\mathrm{exp})}(\omega)\int_0^\infty\frac{d\omega}{2\pi}I_{\mathrm{TM}\to\mathrm{TE}}^{(\mathrm{exp})}(\omega+\Omega)},$$

where the quantities with the superscript "(exp)" denote the experimentally observed spectra. The quantity $R_{\mathrm{TE;TM}}$ equals unity when $I_{\mathrm{TE}\to\mathrm{TM}}^{(\mathrm{exp})}(\omega)\propto I_{\mathrm{TM}\to\mathrm{TE}}^{(\mathrm{exp})}(\omega+\Omega)$. The obtained cross-correlation $R_{\mathrm{TE;TM}}$ is shown in Fig. 4(c). The gray vertical lines in the figure indicate the free spectral range of the WGMs (0 and $\pm62.1$ GHz). The maxima of the cross-correlation at these frequencies qualitatively supports the similarity between the spectra and underlying assumption that the Brillouin scattering process conserves the orbital angular momentum of the photons.

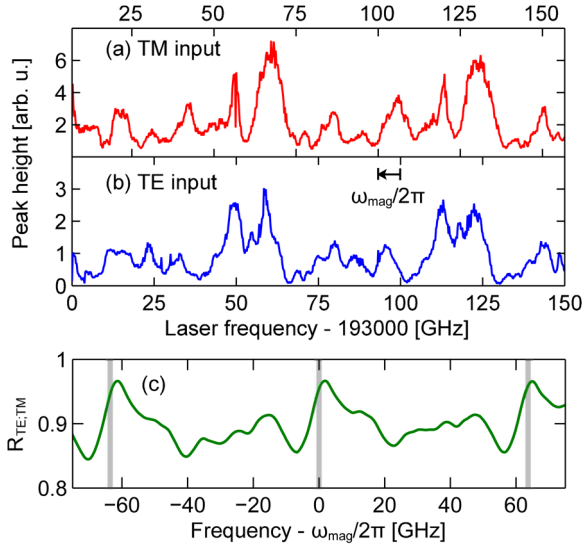


FIG. 4. Peak height of the beat signal vs laser frequency for (a) TM-mode (with an upper horizontal axis) and (b) TE-mode (with a lower one) inputs. (c) Cross-correlation between the two spectra. The gray vertical lines indicate the free spectral range of the WGM.

Note also that the two spectra in Figs. 4(a) and 4(b) do not match the WGM transmission spectra of corresponding polarizations in Fig. 1(b). This discards the simple proportionality between the Brillouin scattering and the transmission spectra and fortifies the claim that the strengths of the Brillouin scattering processes are proportional to $I_{\mathrm{TE}\to\mathrm{TM}}$ and $I_{\mathrm{TM}\to\mathrm{TE}}$, respectively. Complete assignment of the WGMs is needed for a more quantitative understanding of the spectral structure. From this perspective, a WGM resonator with a higher quality factor and a smaller number of relevant spatial modes will be of great help.

For a candidate of a microwave-to-optical-photon quantum transducer, the coupling constant $g$ of the magnon-induced Brillouin scattering and the microwave-to-optical photon conversion efficiency are crucial parameters. The coupling constant is theoretically given by $g^{(\mathrm{theory})}=\mathcal{V}c'\sqrt{2/N_{\mathrm{spin}}}=2\pi\times5.4$ Hz, where $\mathcal{V}$, $c'$, and $N_{\mathrm{spin}}$ are, respectively, the Verdet constant, the speed of light inside the material, and the number of spins in the sample [25]. The experimentally obtained coupling constant $g^{(\mathrm{exp})}$ of $2\pi\times5$ Hz is consistent with the theoretical value [25]. Since the decay rates of the Kittel mode and the WGMs are in the megahertz and gigahertz range, our system is in the weak coupling regime.

In our current setup, the maximum microwave-to-optical photon conversion efficiency is $7\times10^{-14}$ [25], even lower than that in the experiment without a WGM resonator [20]. The main reason for the small value is the frequency mismatch between the frequency difference of the TE and TM WGMs and the Kittel-mode frequency, which can be solved by properly designed WGM resonator geometries. Another reason is the modest quality factors of the WGMs, which can be improved up to the absorption-limited value of $3\times10^6$ [36]. With these improvements, the conversion efficiency will reach $3\times10^{-2}$ [25]. Materials with a larger Verdet constant allow further enhancement by orders of magnitude to make the transduction feasible in the quantum regime.

In conclusion, we observed magnon-induced nonreciprocal Brillouin scattering in a sphere of ferromagnetic insulator material. The phenomena are subject to the unique selection rule imposed by the spin-orbit coupled nature of the WGM photons, the geometrical birefringence of the WGM resonator, and the time-reversal symmetry breaking in the magnon dynamics. The selection rule is also responsible for the sideband asymmetry in the Brillouin scattering process, providing us with a powerful tool to selectively create or annihilate magnons in the Kittel mode

with optical photons. These unique features of the system allow it to serve as an interesting test bed for investigating the interdisciplinary field involving quantum optics and spintronics.

We thank Kohzo Hakuta for his advice. This work was supported by the Project for Developing Innovation System of MEXT, JSPS KAKENHI (Grants No. 26600071, No. 26220601, and No. 15H05461), the Murata Science Foundation, the Inamori Foundation, Research Foundation for Opto-Science and Technology, and NICT.

*alto@qc.rcast.u-tokyo.ac.jp
†usami@qc.rcast.u-tokyo.ac.jp
‡Present address: Research Institute of Electrical Communication, Tohoku University, 2-1-1 Katahira, Aoba-ku, Sendai 980-8577, Japan.

[1] F. Herman, Rev. Mod. Phys. **30**, 102 (1958).
[2] S. Murakami, N. Nagaosa, and S.-C. Zhang, Science **301**, 1348 (2003).
[3] B. A. Bernevig, T. L. Hughes, and S.-C. Zhang, Science **314**, 1757 (2006).
[4] C. Cohen-Tannoudji, J. Dupont-Roc, and G. Grynberg, *Photons & Atoms* (Wiley-VCH, Weinheim, 2004).
[5] M. Onoda, S. Murakami, and N. Nagaosa, Phys. Rev. Lett. **93**, 083901 (2004).
[6] P. V. Kapitanova, P. Ginzburg, F. J. Rodriguez-Fortuño, D. S. Filonov, P. M. Voroshilov, P. A. Belov, A. N. Poddubny, Y. S. Kivshar, G. A. Wurtz, and A. V. Zayats, Nat. Commun. **5**, 3226 (2014).
[7] K. Y. Bliokh, F. J. Rodriguez-Fortuño, F. Nori, and A. V. Zayats, Nat. Photonics **9**, 796 (2015).
[8] J. Petersen, J. Volz, and A. Rauschenbeutel, Science **346**, 67 (2014).
[9] C. Junge, D. O'Shea, J. Volz, and A. Rauschenbeutel, Phys. Rev. Lett. **110**, 213604 (2013).
[10] P. Del'Haye, A. Schliesser, O. Arcizet, T. Wilken, R. Holzwarth, and T. J. Kippenberg, Nature (London) **450**, 1214 (2007).
[11] T. J. Kippenberg, J. Kalkman, A. Polman, and K. J. Vahala, Phys. Rev. A **74**, 051802(R) (2006).
[12] M. Aspelmeyer, T. J. Kippenberg, and F. Marquardt, Rev. Mod. Phys. **86**, 1391 (2014).
[13] M. Goryachev, W. G. Farr, D. L. Creedon, and M. E. Tobar, Phys. Rev. B **89**, 224407 (2014).
[14] T. Satoh, Y. Terui, R. Moriya, B. A. Ivanov, K. Ando, E. Saitoh, T. Shimura, and K. Kuroda, Nat. Photonics **6**, 662 (2012).
[15] T. Satoh, R. Iida, T. Higuchi, M. Fiebig, and T. Shimura, Nat. Photonics **9**, 25 (2015).
[16] X. Zhang, N. Zhu, C.-L. Zou, and H. X. Tang, arXiv: 1510.03545.
[17] J. A. Haigh, S. Langenfeld, N. J. Lambert, J. J. Baumberg, A. J. Ramsay, A. Nunnenkamp, and A. J. Ferguson, Phys. Rev. A **92**, 063845 (2015).
[18] Y. Tabuchi, S. Ishino, T. Ishikawa, R. Yamazaki, K. Usami, and Y. Nakamura, Phys. Rev. Lett. **113**, 083603 (2014).
[19] Y. Tabuchi, S. Ishino, A. Noguchi, T. Ishikawa, R. Yamazaki, K. Usami, and Y. Nakamura, Science **349**, 405 (2015).
[20] R. Hisatomi, A. Osada, Y. Tabuchi, T. Ishikawa, A. Noguchi, R. Yamazaki, K. Usami, and Y. Nakamura, arXiv:1601.03908 [Phys. Rev. B (to be published)].
[21] A. G. Gurevich and G. A. Melkov, *Magnetization Oscillations and Waves* (CRC Press, Boca Raton, FL, 1996).
[22] S. Schiller and R. L. Byer, Opt. Lett. **16**, 1138 (1991).
[23] C. C. Lam, P. T. Leung, and K. Young, J. Opt. Soc. Am. B **9**, 1585 (1992).
[24] S. Schiller, Appl. Opt. **32**, 2181 (1993).
[25] See Supplemental Material at http://link.aps.org/supplemental/10.1103/PhysRevLett.116.223601 for the discussions on the geometrical birefringence, the coupling constant and the conversion efficiency.
[26] Y. R. Shen and N. Bloembergen, Phys. Rev. **143**, 372 (1966).
[27] D. D. Stancil and A. Prabhakar, *Spin Waves: Theory and Applications* (Springer, New York, 2009).
[28] W. Wettling, M. G. Cottam, and J. R. Sandrock, J. Phys. C **8**, 211 (1975).
[29] G. Bahl, M. Tomes, F. Marquardt, and T. Carmon, Nat. Phys. **8**, 203 (2012).
[30] J. H. Kim, M. C. Kuzyk, K. Han, H. Wang, and G. Bahl, Nat. Phys. **11**, 275 (2015).
[31] C. H. Dong, Z. Shen, C. L. Zou, Y. L. Zhang, W. Fu, and G. C. Guo, Nat. Commun. **6**, 6193 (2015).
[32] Z. Yu and S. Fan, Nat. Photonics **3**, 91 (2009).
[33] B. Peng, . K. Ozdemir, F. Lei, F. Monifi, M. Gianfreda, G. L. Long, S. Fan, F. Nori, C. M. Bender, and L. Yang, Nat. Phys. **10**, 394 (2014).
[34] L. Chang, X. Jiang, S. Hua, C. Yang, J. Wen, L. Jiang, G. Li, G. Wang, and M. Xiao, Nat. Photonics **8**, 524 (2014).
[35] *Magneto-Optics*, edited by S. Sugano and N. Kojima, Springer Series in Solid-State Sciences (Springer, New York, 1999).
[36] D. L. Wood and J. P. Remeika, J. Appl. Phys. **38**, 1038 (1967).